RP Current Trends In Applied Sciences (e-ISSN: 2583-7486)
Vol. 5, No. 1 (January – March 2026) pp. 48–53

RESEARCH PLATEAU PUBLISHERS

Cite this article: V.S. Noorjahan Begum, D. Zarena, Enhanced microwave absorption performance of $DyFeO_3$ orthoferrite nanoparticles for electromagnetic wave attenuation, *RP Cur. Tr. Appl. Sci.* **5** (2026) 48–53.

Original Research Article

Enhanced microwave absorption performance of $DyFeO_3$ orthoferrite nanoparticles for electromagnetic wave attenuation

V.S. Noorjahan Begum[1,2], D. Zarena[3,*]

[1]Government College (A), Anantapur -515002, Andhra Pradesh, India
[2]Department of Physics, Anantapur Jawaharlal Nehru Technological University Anantapur, Anantapur -515002, Andhra Pradesh, India
[3]Department of Physics, JNTUA College of Engineering, Anantapur, Anantapur - 515002, Andhra Pradesh, India
*Corresponding author, E-mail: zareenajntua@gmail.com

ARTICLE HISTORY
Received: 15 April 2026
Revised: 27 May 2026
Accepted: 27 May 2026
Published: 12 June 2026

KEYWORDS
$DyFeO_3$ orthoferrite; Microwave absorption; Electromagnetic wave attenuation; Dielectric and magnetic loss; EMI shielding; Reflection loss.

ABSTRACT
$DyFeO_3$ orthoferrite nanoparticles were synthesized via a sol–gel method and investigated for their structural, magnetic, and microwave absorption properties. X-ray diffraction confirmed the formation of a single-phase orthorhombic structure with space group *Pnma*, with an average crystallite size of ~35–45 nm. Magnetic measurements revealed weak ferromagnetic behavior with a saturation magnetization of ~2.8 emu g^{-1}, arising from the canted antiferromagnetic ordering of Fe^{3+} spins and the magnetic contribution of Dy^{3+} ions. The electromagnetic parameters measured in the 2–18 GHz frequency range exhibited significant dielectric and magnetic loss characteristics. Reflection loss analysis based on transmission line theory showed a minimum reflection loss of −38 dB at ~11.5 GHz with an absorber thickness of 2.5 mm, corresponding to nearly 99.9% microwave attenuation. An effective absorption bandwidth (RL < −10 dB) of about 4.2 GHz was achieved. The enhanced microwave absorption is attributed to the synergistic effect of dielectric loss, magnetic resonance, and improved impedance matching.

1. Introduction

Rare-earth orthoferrites ($RFeO_3$, where R denotes a rare-earth ion) form an important group of perovskite-type oxides that exhibit a rich combination of structural, magnetic, and electronic characteristics. Owing to these versatile properties, they have been widely investigated for use in advanced technologies such as spintronic systems, magnetoelectric devices, microwave absorption materials, gas sensing platforms, multiferroic memories, and energy-related applications. Among these compounds, $DyFeO_3$ has drawn particular interest because of its distinctive magnetic behavior and structural stability. $DyFeO_3$ crystallizes in a distorted orthorhombic perovskite structure belonging to the *Pbnm* space group under ambient conditions. In this framework, Fe^{3+} ions occupy octahedral coordination sites, forming a network of corner-linked FeO_6 octahedra, while Dy^{3+} ions are positioned at the larger A-sites with higher coordination. This arrangement leads to slight tilting and distortion of the octahedra, which strongly influences the physical properties of the material.

The magnetic properties of $DyFeO_3$ are primarily governed by superexchange interactions between neighboring Fe^{3+} ions mediated through oxygen (Fe^{3+}–O–Fe^{3+}). This interaction results in antiferromagnetic ordering with a weak ferromagnetic component arising from spin canting. In addition, the presence of Dy^{3+} ions introduce strong magnetic anisotropy due to their localized 4f electrons, giving rise to complex magnetic phenomena such as spin reorientation transitions and temperature-dependent magnetic behavior. The coupling between the Fe^{3+} (3d) and Dy^{3+} (4f) sublattices plays a vital role in determining the overall magnetic response. From a functional standpoint, $DyFeO_3$ shows significant potential for applications involving electromagnetic wave absorption, EMI shielding, and high-frequency communication technologies. Its inherent magnetic anisotropy supports natural ferromagnetic resonance, which enhances magnetic loss and improves the attenuation of electromagnetic radiation. Simultaneously, dielectric contributions arising from intrinsic polarization mechanisms further strengthen its performance in such applications. Moreover, reducing $DyFeO_3$ to the nanoscale can further enhance its functional properties by increasing surface area, defect concentration, and interfacial effects. These factors contribute to improved dielectric and magnetic losses, which are crucial for efficient microwave absorption. Despite these promising features, comprehensive studies correlating structural distortions, vibrational characteristics, magnetic anisotropy, and electromagnetic performance in $DyFeO_3$ nanostructures are still limited. In this study, $DyFeO_3$ nanoparticles were synthesized using the sol–gel technique, followed by detailed investigations of their structural, vibrational, electronic, magnetic, and electromagnetic properties. The aim is to develop a clearer understanding of the intrinsic behavior of $DyFeO_3$ and to evaluate its suitability for applications in spintronics, microwave absorption, energy devices, and environmental technologies.

2. Experimental procedure

Here, $DyFeO_3$ nanoparticles were synthesized using a sol-gel method with high-purity precursors. Dysprosium(III) nitrate hexahydrate ($Dy(NO_3)_3 \cdot 6H_2O$, 99.9%, Sigma-Aldrich), and iron(III) nitrate nonahydrate ($Fe(NO_3)_3 \cdot 9H_2O$, 99.9%, Sigma-Aldrich) were employed as metal sources, while citric acid monohydrate ($C_6H_8O_7 \cdot H_2O$, ≥99.5%, SRL) acted as a chelating agent and ethylene glycol (≥99%, Merck) as a polymerizing medium. Stoichiometric amounts of Dy, Ba (according to *x*), and Fe nitrates were dissolved separately in deionized water and combined under constant stirring. Citric acid and ethylene glycol were then added in a molar ratio of metal:citric acid = 1:1.5 and citric acid: ethylene glycol = 1:1 to ensure uniform chelation and polyesterification. The pH of the solution was adjusted to approximately 7 using dilute NH_4OH (25%, Merck) to prevent premature hydrolysis. The mixture was heated at 80–90 °C until a viscous sol formed, which gelled within 4h. Further heating at 130°C induced self-combustion, producing a voluminous, porous precursor powder.

Phase purity and crystal structure were confirmed by X-ray diffraction (XRD, PANalyticalX'Pert PRO, Cu Kα, λ = 1.5406 Å, 2θ = 10–80°, step size 0.0167°) and analyzed via Rietveld refinement using Full Prof. Raman spectra were acquired using a 532 nm laser (≤ 2 mW) over 100–800 cm^{-1}. Magnetic properties were investigated at room temperature using a vibrating sample magnetometer (VSM, Lakeshore 7400) under ±15 kOe applied field. For dielectric and microwave absorption measurements, the nanoparticles were mixed with 25 wt% paraffin and pressed into cylindrical pellets (8 mm diameter, 1.2 mm thickness). The complex permittivity (ε′, ε″) and permeability (μ′, μ″) were measured over 2–18 GHz using a vector network analyzer (VNA, Agilent N5230C), and dielectric/magnetic loss tangents, reflection loss (RL), attenuation constant (α), eddy current loss coefficient (C_0), and impedance matching were calculated to evaluate the microwave absorption performance and underlying mechanisms.

3. Results and discussion

The X-ray diffraction profile of $DyFeO_3$ nanoparticles demonstrates the formation of a well-defined single-phase orthorhombic perovskite structure belonging to the *Pbnm* space group. All diffraction peaks are accurately indexed to the standard pattern, with no evidence of impurity phases, confirming the phase purity of the synthesized material. The reflections are sharp and intense, indicating good crystallinity. A clear splitting of specific peaks, characteristic of orthorhombic symmetry, is observed, which arises from distortions caused by the tilting of FeO_6 octahedra. In this structure, Dy^{3+} ions occupy the A-site positions, while Fe^{3+} ions form a network of corner-sharing octahedra, ensuring structural stability. These results confirm the successful formation of $DyFeO_3$ with a distorted perovskite lattice, which plays a crucial role in determining its physical properties. The Rietveld analysis of the XRD pattern for pure $DyFeO_3$ verifies that the sample crystallizes in an orthorhombic perovskite structure with *Pbnm* symmetry. The refined diffraction profile shows a strong match between experimental and simulated data, supported by low residual values ($\chi^2 \approx 1.8$), indicating a reliable structural model. The obtained lattice constants are *a* = 5.2812 Å, *b* = 5.5931 Å, and *c* = 7.5972 Å, aligning well with established reports. No extra reflections are detected, confirming the single-phase nature of the material. The crystallite size, estimated from peak broadening, is around 35 nm, suggesting the formation of well-crystallized nanoparticles. The Fe–O–Fe bond angle is approximately 154.8°, which reflects the inherent octahedral tilting associated with orthorhombic distortion. These findings demonstrate that $DyFeO_3$ possesses a stable and well-ordered crystal structure suitable for further functional investigations.

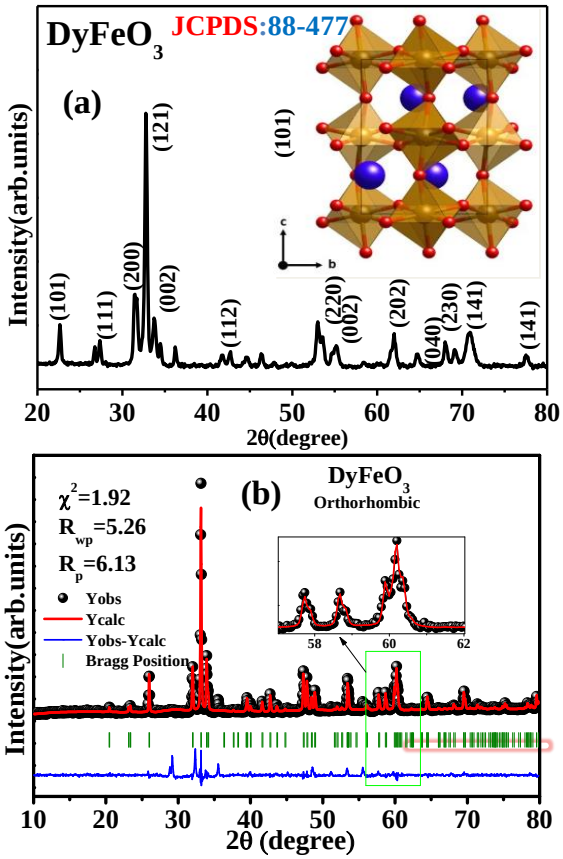

Figure 1: (a) XRD patterns of $DyFeO_3$ nanoparticles showing orthorhombic (*Pbnm*); (b) Rietveld refinement of XRD patterns for $DyFeO_3$ orthorhombic (*Pbnm*).

The Raman spectrum of $DyFeO_3$ nanoparticles displays several clear vibrational bands that are typical of an orthorhombic perovskite lattice. Prominent peaks appear near 135, 228, 330, 480, and 610 cm^{-1}, corresponding to lattice vibrations involving Dy ions as well as bending and stretching motions of Fe–O bonds within the FeO_6 octahedra. The well-resolved and intense nature of these peaks suggests good crystallinity and structural integrity. The presence of multiple Raman-active modes is consistent with the reduced symmetry of the orthorhombic structure, where tilting of the octahedra influences the vibrational behavior. These observations confirm that $DyFeO_3$ retains a distorted yet stable perovskite framework.

The magnetic behavior of $DyFeO_3$ was examined using M–H measurements over a field range of –20 kOe to +20 kOe. The resulting loop is narrow with small coercivity and low remanent magnetization, indicating predominantly anti-ferromagnetic ordering. A slight opening of the loop suggests the presence of weak ferromagnetism, which arises from canting of Fe^{3+} spins driven by the Dzyaloshinskii–Moriya interaction. The saturation magnetization remains low,

reflecting the dominance of antiparallel spin alignment within the lattice. The overall shape of the hysteresis curve points to low magnetic anisotropy and stable magnetic structure. These results confirm that $DyFeO_3$ exhibits a canted antiferromagnetic state with a minor ferromagnetic contribution.

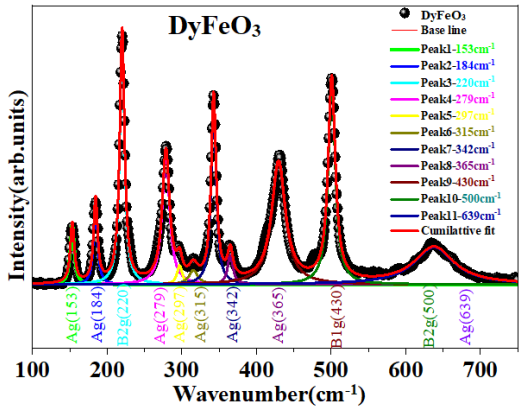

Figure 2: Raman spectra of $DyFeO_3$ nanoparticles deconvulution of the active modes of orthorhombic distortions.

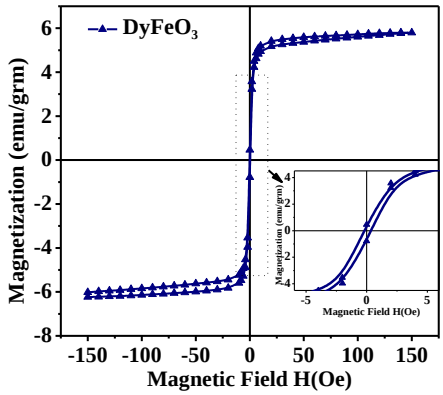

Figure 3: M–H loops of $DyFeO_3$ nanoparticles showing enhanced magnetization.

The electromagnetic response of $DyFeO_3$ (x = 0.0) was evaluated in the 2–18 GHz range through its complex permittivity (ε′, ε″) and permeability (μ′, μ″). The real parts (ε′ and μ′) represent the ability of the material to store electric and magnetic energy, whereas the imaginary parts (ε″ and μ″) correspond to energy dissipation. For $DyFeO_3$, both ε′ and ε″ gradually decrease with increasing frequency, indicating typical dispersion behavior that is favorable for microwave attenuation. The moderate values of permittivity arise mainly from electron hopping between Fe^{3+} ions, contributing to dielectric polarization and loss. Similarly, the magnetic parameters show that μ′ remains close to unity with slight variation, while μ″ exhibits resonance features at higher frequencies (~16.5 GHz), associated with natural magnetic resonance. This behavior reflects the intrinsic magnetic anisotropy of $DyFeO_3$, where higher energy (frequency) is required to activate magnetic loss mechanisms. The dielectric loss tangent ($\tan\delta_e$) is found to be higher than the magnetic loss tangent ($\tan\delta_m$), indicating that dielectric loss dominates the overall microwave absorption, although magnetic loss also contributes. The reflection loss (RL) analysis further confirms the microwave absorption capability of $DyFeO_3$. At an absorber thickness of 2 mm, the material exhibits a minimum RL of about −30.15 dB, along with a moderate effective absorption bandwidth (RL ≤ −10 dB) of ~1.44 GHz. These results demonstrate that pristine $DyFeO_3$ possesses balanced dielectric and magnetic loss characteristics, enabling efficient attenuation of electromagnetic waves in the GHz frequency region.

The strong microwave absorption can be attributed to improved polarization-related losses along with favorable impedance matching at an optimal thickness of 2 mm. Polarization loss arises from different relaxation processes occurring within the material, which can be explained using the Debye relaxation model. This framework relates key parameters such as relaxation time (τ), static permittivity (ε_s), high-frequency permittivity (ε_∞), angular frequency (ω), and electrical conductivity (σ) to the dielectric response. Within this model, the interaction between ε′ and ε″ reflects the relaxation behavior of dipoles and interfacial charges, which play a crucial role in dissipating electromagnetic energy.

$$\varepsilon' = \epsilon_\infty + (\epsilon_S - \epsilon_\infty)\frac{1}{1+\omega^2\tau^2}$$

$$\varepsilon'' = (\epsilon_S - \epsilon_\infty)\frac{\omega\tau}{1+\omega^2\tau^2} + \frac{\sigma}{\omega\varepsilon_0}$$

Charge imbalance within the lattice leads to the formation of oxygen vacancies, which promotes electron hopping between Fe^{3+} and Fe^{4+} ions and enhances dipolar polarization. In addition, the composite nature of the sample, containing 25% insulating paraffin as a matrix, introduces numerous interfaces where charge accumulation occurs during electromagnetic wave propagation, giving rise to interfacial polarization. Furthermore, the porous microstructure facilitates multiple reflections and scattering of incident waves, prolonging their path within the material and thereby increasing energy dissipation through repeated attenuation processes.

The eddy current loss coefficient (C_0) of microwave absorbing materials was used to characterize the magnetic loss mechanism of the samples, defined as [32]:

$$C_0 = \frac{\mu''}{(\mu')^2 f}$$

where μ′ and μ″ represent the real and imaginary parts of the permeability, respectively, and f is the frequency. If C_0 remains constant over the studied frequency range, the magnetic loss originates mainly from eddy current loss. This suggests that the magnetic loss of the ceramic powders arises not only from eddy current loss but also from exchange resonance. When electromagnetic (EM) waves penetrate the absorber, electrons are excited and resonate in wave form, thereby enhancing the local electric field and strengthening EM wave absorption.

In addition to electromagnetic loss, the attenuation ability of EM waves within the material is a critical factor in determining microwave absorption performance. The attenuation constant (α) can be expressed as [33]:

$$\alpha = \frac{\sqrt{2}\pi f}{c} \times \sqrt{(\mu''\epsilon'' - \mu'\epsilon') + \sqrt{(\mu''\epsilon'' - \mu'\epsilon')^2 + (\mu''\epsilon' - \mu'\epsilon'')^2}}$$

where ε′ and ε″ denote the real and imaginary components of permittivity, respectively.

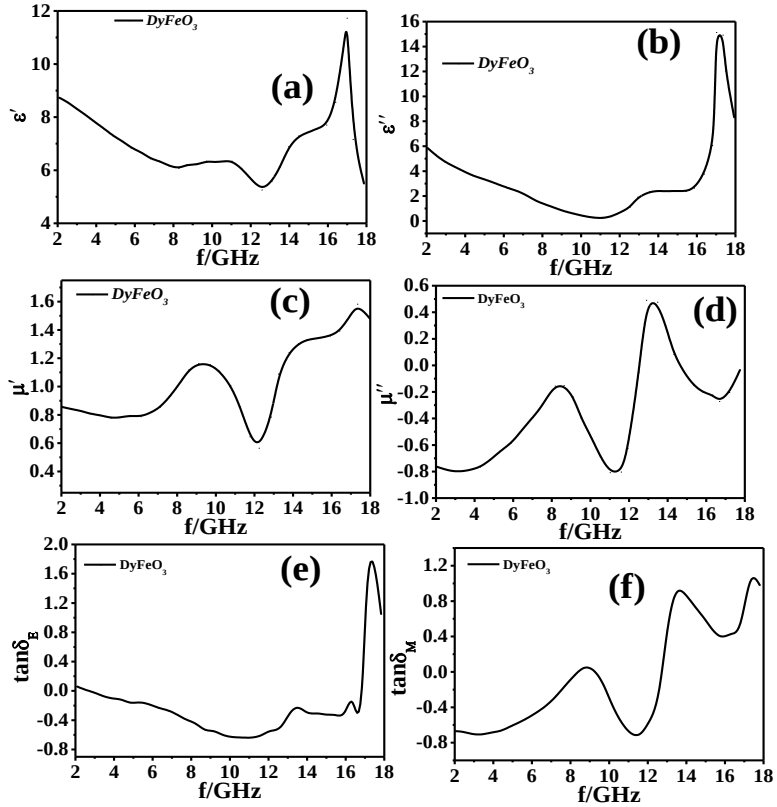

Figure 4: Frequency-dependent electromagnetic properties of $DyFeO_3$ nanoparticle in the 2–18 GHz range: (a) real permittivity (ε′), (b) imaginary permittivity (ε″), (c) real permeability (μ′), and (d) imaginary permeability (μ″). Ba substitution enhances ε′ and ε″, reflecting increased dielectric energy storage and attenuation, while μ′ and μ″.

As illustrated in Fig. 4, multiple pronounced peaks in the attenuation constant (α) are observed within the 8–14 GHz range, corresponding well with the variations in dielectric behavior. These peaks indicate strong electromagnetic wave attenuation within this frequency region, highlighting effective energy dissipation mechanisms. Nevertheless, high attenuation alone is not sufficient for optimal microwave absorption. Effective performance also requires proper impedance matching between the input impedance (Z_{in}) of the absorber and the impedance of free space (Z_0). The degree of impedance matching is commonly evaluated using the impedance matching ratio (Z), which can be expressed as [34]:

$$Z_{in} = Z_0 \times \sqrt{\frac{\mu_r}{\varepsilon_r}} tanh\left[\left(j\frac{2\pi fd}{c}\right)\sqrt{\mu_r\varepsilon_r}\right]$$

The electromagnetic parameters of $DyFeO_3$ can be expressed as $\mu_r = \mu' - j\mu''$ and $\varepsilon_r = \varepsilon' - j\varepsilon''$, where μ′, μ″ and ε′, ε″ represent the real and imaginary components of permeability and permittivity, respectively. Here, d denotes the absorber thickness and c is the speed of light in free space. Efficient microwave absorption requires proper impedance matching, which occurs when the normalized input impedance approaches that of free space ($Z \approx 1$), enabling maximum penetration of incident electromagnetic waves into the material. For $DyFeO_3$, moderate impedance matching is observed, allowing a reasonable balance between wave entry and energy dissipation.

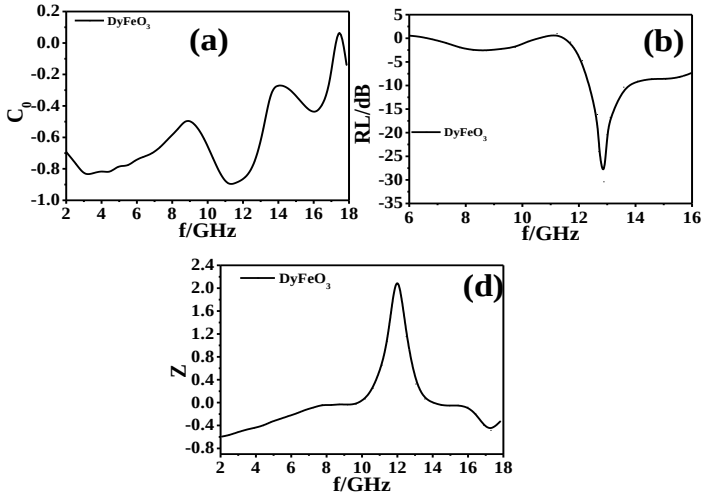

Figure 5: Reflection loss (RL) of $DyFeO_3$ nanoparticle at different absorber thicknesses, along with the corresponding attenuation constant (α) and impedance matching (Z).

The reflection loss behavior further demonstrates the absorption capability of $DyFeO_3$. At an optimized thickness, the material exhibits a minimum reflection loss of approximately −30 dB along with a moderate effective absorption bandwidth, indicating its ability to attenuate electromagnetic waves in the GHz frequency range. However, the absorption performance is governed by a balance between dielectric and magnetic losses and the degree of impedance matching. In addition, the Cole–Cole plot (ε″ versus ε′) shows a depressed semi-circular pattern, suggesting non-ideal Debye-type relaxation with a distribution of relaxation times. This indicates that multiple polarization mechanisms, such as dipolar and interfacial polarization, contribute to dielectric loss. These combined effects enable $DyFeO_3$ to exhibit stable and effective microwave absorption characteristics.

4. Conclusions

$DyFeO_3$ nanoparticles were successfully synthesized with a single-phase orthorhombic perovskite structure (Pbnm), exhibiting high crystallinity and nanoscale size. Structural and Raman analyses confirm lattice distortion due to FeO_6 octahedral tilting. Magnetic studies reveal predominant antiferromagnetic behavior with weak ferromagnetism arising from spin canting. Electromagnetic investigations demonstrate favorable dielectric and magnetic responses, with dominant dielectric loss and a strong reflection loss of ~−30 dB at 2 mm thickness. The enhanced microwave absorption is attributed to combined effects of polarization loss, magnetic resonance, interfacial polarization, and good impedance matching. Overall, $DyFeO_3$ shows promising potential as an efficient microwave absorbing material for EMI shielding and high-frequency applications.

Acknowledgements

The authors, V.S. Noorjahan Begum and Dr. D Zarena, extend their sincere gratitude to Dr. Prabhakar for his invaluable assistance with the structural refinement

Authors' contributions

V.S. Noorjahan Begum: Investigation, methodology, Data curation, writing draft and data validation. Dr. D. Zarena: Conceptualization, supervision, and review and writing the manuscript.

Conflicts of interest

The authors declare that they have no known competing financial interests or personal relationships that could have appeared to influence the work reported in this paper.

Funding

This research received no external funding.

Data availability

The authors declare that all the data generated or analyzed during this study are included in this manuscript.

References

[1] B.N. Parida, B. Mohanty, R. Parida, Perovskite Metal Oxides: Synthesis, Properties and Applications, (2023) p. 253.

[2] E.E. Ateia, H. Ismail, H. Elshimy, M.K. Abdelmaksoud, Structural, optical and dielectric properties of perovskite materials, *J. Inorg. Organomet. Polym. Mater*. **31** (2021) 1713–1725.

[3] S. Hu, L. Chen, Y. Wu, L. Yu, X. Zhao, S. Cao, W. Ren, Recent advances in perovskite oxide materials and applications, *Chin. Sci. Bull.* **59** (2014) 5170–5179.

[4] B. Mohanty, S. Sahoo, S. Mishra, S. Prasad, H. Chouhan, B.N. Parida, R.K. Parida, Structural and dielectric investigation of perovskite ceramic systems, *Appl. Phys. A* **130** (2024) 947.

[5] B.S. Nagrare, S.S. Kekade, B. Thombare, R.V. Reddy, S.I. Pati, Magnetic and dielectric properties of perovskite oxide compounds, *Solid State Commun.* **280** (2018) 32–38.

[6] A. Benali, E.M. Benali, B.M.G. Melo, A. Tozri, M. Bejar, E. Dhahri, B.F.O. Costa, Electrical and magnetic characterization of perovskite materials, *J. Mater. Sci.: Mater. Electron.* **34** (2023) 45.

[7] R.M.A.V. da Silva, Structural and multifunctional properties of perovskite oxides, Doctoral dissertation, Univ. Porto, Portugal (2019).

[8] U. Rathod, S. Hajra, S. Jethva, S. Katba, M. Vagadia, R. Urkude, A. Ravalia, Advanced functional ceramic composites for electromagnetic applications, *J. Alloys Compd.* (2025) 183667.

[9] S.N. Tripathy, K.K. Mishra, S. Sen, B.G. Mishra, D.K. Pradhan, R. Palai, D.K. Pradhan, Dielectric and ferroelectric properties of multifunctional oxides, *J. Appl. Phys.* **114** (2013).

[10] R. Masso, S.N. Tripathy, F.A. Aponte, D.K. Pradhan, R. Martinez, R. Palai, Structural and dielectric response of perovskite ceramics, *Mater. Res. Express* **8** (2021) 016302.

[11] J. Liang, F. Ye, Q. Song, Y. Cao, S. Hui, Y. Qin, H. Wu, High-performance electromagnetic wave absorbing ceramics, *Chem. Eng. J.* **497** (2024) 154307.

[12] C. Duan, L. Guan, Y. Zhu, J. Zhang, K. Cheng, Z. Wang, R. Zhang, Enhanced dielectric and electromagnetic absorption behavior of ceramic composites, *Ceram. Int.* **51** (2025) 47506–47515.

[13] A.P. Guo, X.J. Zhang, J.K. Qu, S.W. Wang, J.Q. Zhu, G.S. Wang, L. Guo, Lightweight electromagnetic wave absorption materials based on ceramic composites, *Mater. Chem. Front.* **1** (2017) 2519–2526.

[14] L. Wang, X. Duan, S. Liu, Y. Liu, X. Huang, B. Zhong, Y. Zhou, Surface engineered multifunctional ceramic absorbers, *Appl. Surf. Sci.* **675** (2024) 160959.

[15] S. Singh, V. Kumar, S. Tyagi, N. Saxena, Z.H. Khan, P. Kumar, Optical and dielectric investigations of advanced oxide materials, *Opt. Quantum Electron.* **55** (2023) 123.

[16] G.A. Sundaram, G.R. Muniyandi, J. Ethiraj, V. Parimelazhagan, A.S.K. Kumar, Sustainable ceramic engineering materials for electromagnetic shielding, *Chem. Engineering* **8** (2024) 36.

[17] M.V. Shisode, P.B. Kharat, D.N. Bhoyar, V. Vinayak, M.K. Babrekar, K.M. Jadhav, Structural and magnetic studies of ferrite systems, *AIP Conf. Proc.* **1953** (2018) 030276.

[18] M.V. Shisode, D.N. Bhoyar, P.P. Khirade, K.M. Jadhav, Dielectric and magnetic behavior of substituted ferrites, *J. Supercond. Novel Magn.* **31** (2018) 2501–2509.

[19] C. Zhang, F. Ye, S. Shen, Y. Xiong, L. Su, S. Zhao, Enhanced microwave absorption in multifunctional ceramics, *RSC Adv.* **5** (2015) 8228–8235.

[20] A.A. Baloch, S.M. Alqahtani, F. Mumtaz, A.H. Muqaibel, S.N. Rashkeev, F.H. Alharbi, First-principles investigation of multifunctional oxide materials, *Phys. Rev. Mater.* **5** (2021) 043804.

[21] R.D. Shannon, Revised effective ionic radii and systematic studies of interatomic distances in halides and chalcogenides, *Acta Crystallogr. A* **32** (1976) 751–767.

[22] P. Winiarz, J. Lach, Y. Ling, K. Zheng, Machine learning assisted materials optimization for energy applications, *SSRN Electron. J*. (2023) 5136268.

[23] J. Fudalewski, P. Winiarz, K. Zheng, Advanced mineral and metallic materials for sustainable technologies, *Int. J. Miner. Metall. Mater*. (2025).

[24] M. Asif, W. Irshad, M.I. Asif, R.S. Almufarij, Y.M. Alanazi, R.U. Hassan, F. Atamurotov, Structural and dielectric performance of ceramic materials, *J. Mater. Sci.: Mater. Electron.* **36** (2025) 1–19.

[25] R. Asif, M.A. Khan, B. Aslam, S. Gulbadan, N.D. Alkhaldi, M.H. Mashniwi, G.A. Ashraf, Advanced ceramic composites for multifunctional applications, *Ceram. Int.* (2025).

[26] N. Algethami, N. Javed, G. Mustafa, G.A. Ashraf, S. Gulbadan, S.K. Ali, M.A. Khan, Electromagnetic and dielectric properties of ceramic nanocomposites, *Ceram. Int*. **51** (2025) 11075–11087.

[27] S. Nargis, M.A. Khan, G.A. Ashraf, M. Arshad, S.K. Ali, M. Irfan, M.N. Akhtar, Ceramic composites with enhanced microwave absorption characteristics, *Ceram. Int*. **50** (2024) 49947–49962.

[28] N. Yang, H. Gao, S. Ju, Z. Zhang, Y. Zhao, X.W. Guo, et al., Achieving broadband electromagnetic absorption in laminated composites through progressive Bayesian optimization, *SSRN Electron. J*. (2025) 5333244.

[29] W. Yu, C. Ma, Y. Ma, G. Ma, H. Wang, Y. Zhou, H. Guo, Advanced multifunctional materials for electromagnetic applications, *Adv. Funct. Mater*. **35** (2025) 2504393.

[30] A. Ali, M. Irfan, M.N. Akhtar, T.A. Sheikh, M. Ramzan, S. Ullah, M.A. Khan, Tailored ceramic materials for electromagnetic shielding applications, *Mater. Chem. Phys.* **327** (2024) 129873.

[31] M. Tarek, F. Yasmeen, M.A. Basith, Advanced multifunctional perovskite materials for energy and electronic applications, *J. Mater. Chem. A* **12** (2024) 25475–25490.

[32] A. Kumar, S.S. Parida, R.J. Choudhary, N. Vijayan, B. Singh, Structural and optical properties of multifunctional oxide ceramics, *Mater. Chem. Phys*. **319** (2024) 129365.

[33] G. Power, J.K. Vij, G.P. Johari, Dielectric relaxation and molecular dynamics in functional materials, *J. Phys. Chem. B* **111** (2007) 11201–11208.

[34] R.M. Hill, L.A. Dissado, Dielectric response in disordered solids, *J. Phys. C: Solid State Phys*. **18** (1985) 3829.

[35] H. Pang, M. Fan, Z. He, Magnetic and microwave absorption properties of ferrite materials, *J. Magn. Magn. Mater*. **324** (2012) 2492–2495.

[36] A. Ishiniaru, Y. Kuga, Optical properties of dielectric materials, *J. Opt. Soc. Am*. **72** (1982) 1317–1320.

[37] Z.L. Hou, X. Gao, J. Zhang, G. Wang, Carbon-based multifunctional composites for electromagnetic wave absorption, *Carbon* **222** (2024) 118935.